SILVER ION IMPLANTATION AND ANNEALING IN CVD SILICON CARBIDE: THE EFFECT OF TEMPERATURE ON SILVER MIGRATION

Heather J. MacLean [a], Ronald G. Ballinger [a]

([a] Massachusetts Institute of Technology, Cambridge, Massachusetts, USA)

ABSTRACT

The effect of temperature on the migration of silver in CVD β-SiC has been studied using ion-implantation. Silver ions with were implanted in β SiC using the ATLAS accelerator facility at the Argonne National Laboratory. Ion beams with energies of 93 and 161 MeV were used to achieve deposition with peak concentrations at approximately 9 and 13 μm depth respectively. As-implanted samples were then annealed at 1500°C for 210 and 480 hours. XPS, SEM, TEM, STEM, and optical methods were used to analyze the material before and after annealing. Silver concentration profiles were determined using XPS before and after annealing. STEM and SEM equipped with quantitative chemical analysis capability were used to more fully characterize the location and morphology of the silver before and after annealing. The results show that, within the uncertainty of measurement techniques, there is no silver migration, either inter or intra-grannular, for the times and temperature studied. Additionally, the silver was observed to phase separate within the SiC after annealing. The irradiation damage from the implantation process resulted in a three-layer morphology in the as-implanted condition: (1) a layer of unaltered SiC followed by (2) a layer of crystallized SiC, followed by (3) an amorphized layer which contained essentially all of the implanted silver. After annealing the layer structure changed. Layer 1 was unaltered. Layer 2 recrystallized to form an epitaxial (columnar) layer. Layer 3 recrystallized to form a fine grain equiaxed layer. The results of this work does not support the long held assumption that silver migrates by grain boundary diffusion in CVD SiC used for gas reactor coated particle fuel.

Key Words: Ion Implantation, Silver Diffusion, Silicon Carbide

1. INTRODUCTION

The standard TRISO coated particle fuel design used for high temperature gas reactor fuel consists of a fuel kernel surrounded by successive layers of: (1) low density pyrocarbon, (2) high density pyrocarbon, (3) silicon carbide (SiC) and (4) high density pyrocarbon. The SiC layer serves as the main barrier to fission product release. Although most fission products, such as cesium, iodine, xenon, and krypton, are retained by the combination of pyrocarbon and SiC layers, previous observations of silver release during fuel testing and operation raises concerns that the SiC layer may not be as effective for silver. Silver release from silicon carbide coated fuel increases the total activity levels in the primary circuits of high-temperature gas reactors which makes maintenance more difficult and costly.

Silver release has been observed on apparently intact fuel, suggesting that silver is transported through intact silicon carbide layers. In many cases, experimental measurements of silver release was observed to exhibit a temperature dependence that has been interpreted as a sign of a diffusive mechanism. In most cases, however, silver release has been reported only for either a batch of fuel particles or an entire fuel element, leaving uncertainties about individual particle performance. In cases where fission product release from individual particles has been measured, and where individual coated particle characteristics and radiation environments have been essentially identical, silver release, as characterized by rates, timing, and release fractions, has been highly variable. In some cases the release fraction has varied from 0% to 100% among nominally identical particles. An additional complicating factor is that previously reported release data has, in fact, only been analyzed with the assumption that diffusion was the actual release mechanism. It would follow that if a thermally activated process such as diffusion were controlling transport and release, then for a given set of nominally identical conditions, there would be a

common temperature dependence observed. The absence of such a dependence would seem to eliminate diffusion as the dominant release mechanism. To date, specific silver concentration profiles, characteristic of diffusion in silicon carbide, have not been reported.

In previous work, Nabielek et al. implanted low energy silver ions into SiC disk samples and measured the concentration profile before and after annealing [1]. They observed no change in the silver concentration profile after exposure for 30 min at 1180°C and reported a "maximum" value for the diffusion coefficient of approximately 1 x 10^{-19} m^2/s based on assuming that the actual migration was just below the minimum sensitivity of their detection method. Nabielek et al. attributed their results to silver ions becoming trapped in silicon carbide grains during implantation and not being able to diffuse along grain boundaries.

Although the results of Nabielek et al. were inconclusive, their implantation experiment was conducted at a very low temperature, 1180°C, with respect to the SiC melting point of 2830°C and for a very short time. Assuming that a vacancy transport mechanism would be operative one would not expect significant matrix diffusion below approximately half of the absolute melting temperature. Grain boundary diffusion would be of the order 10^3 faster than matrix diffusion, but even if this were the transport mechanism the rate would be very slow. For these reasons one would not expect that even if a vacancy mechanism were operative, that Nabielek would have observed it. Although there are no directly measured diffusion data for silver reported in the literature in SiC, there are data for other atoms of similar size. Data from Bernhok etal. for aluminum and gallium in 6H-SiC indicate diffusion coefficients in the range 10^{-18}-5 x 10^{-16} m^2/s in the temperature range 1800-2300°C [2]. Extrapolation of these data to lower temperatures yields values of approximately 10^{-19} cm^2/s and 10^{-24} cm^2/s at 1500°C and 1100°C, respectively. In contrast, reported values of diffusion coefficients, assumed to be grain boundary transport, from silver release measurements have been of the order 10^{-17} m^2/s and 5×10^{-13} m^2/s at 1000°C and 1800°C, respectively. Thus, there appears to be a significant discrepancy between observed release-based derived diffusion coefficients and what might be considered as likely based on comparison, albeit only approximate, with other similar size atoms, even if grain boundary diffusion is assumed.

Because of the potential significance that a more detailed understanding of the migration of silver in SiC could have for the design of advanced coated particle fuel systems, a program has been under way for the past two years to develop this understanding. Initial results of this program have been reported elsewhere [3,4]. As a part of this program, experimental measurement of the diffusion coefficient of silver in SiC has been a primary goal. Ion implantation experiments were conducted to investigate silver behavior in SiC at higher temperature-1500°C, a temperature more likely to facilitate silver diffusion, and to observe silver migration starting with a known and measurable concentration. This paper reports on the results of this program.

2. EXPERIMENTAL

2.1. MATERIALS

Flat plate, CVD SiC, 0.3 cm thick, was the starting material for the ion implantation experiments. The material was obtained from Coorstek, Inc. The reported density was 3.21 gm/cm^3 with grain sizes in the range of 3-10 μm, preferentially oriented in the direction perpendicular to the SiC surface. X-ray diffraction (XRD) analysis on a polished SiC sample confirmed that the material was crystalline β-SiC with a strong preferred orientation such that the (111) planes were parallel to the surface.

Each ion implantation sample was cut to 5 × 5 × 0.3 cm. One 5 × 5 cm face of each sample was polished to a mirror finish with a mean surface roughness, Ra, of 0.005 μm as measured by a Zygo interference microscope. A flat and uniform initial SiC surface ensured the best possible implanted silver profile.

2.2. ION IMPLANTATION

The goals of the ion implantation studies were to implant a measurable quantity of silver in silicon carbide and, moreover, to implant the silver deep enough so that it would not migrate out of the sample during subsequent annealing. Based on silver diffusion coefficients reported in the literature by Amian and Stöver, it was expected that the silver could diffuse farther than 10 μm in as little as 10 hours at 1500°C with the peak concentration dropping to less than 2% of its original value [5]. To prevent excessive silver loss during annealing and to avoid surface effects resulting from the mechanical polishing process, the silver needed to be implanted at a depth of approximately 9-15 μm. Calculations using the SRIM (Stopping and Range of Ions in Matter) code package indicated that ion beam energies on the order of 90-160 MeV were necessary to achieve implantation depths in this range [6].

The silver ion implantation was performed at the ATLAS facility at the Argonne National Laboratory using the positive-ion injector (PII) to create the silver beam. PII consists of three major subsystems: an electron cyclotron resonance (ECR) ion source and high-voltage platform, a 12-MHz beam bunching system, and a 12-MV super conducting LINAC accelerator. The PII ECR source is a 10-GHz electron cyclotron resonance ion source mounted on a high-voltage platform. The beam bunching system compresses the beam into narrow time packets, allowing the LINAC to accelerate the ion beam without introducing significant energy spread. The super conducting resonators in the PII LINAC accelerate the ion beam from the low velocity provided by the PII ECR to the higher velocity required for injection into the remainder of ATLAS.

Two batches of samples were irradiated at ATLAS. The first batch contained samples designated 1, 2a, and 2b. Silver ions with a total energy of 161 MeV and a charge state of +18 were implanted at a mean range of 12.8 μm with a peak at 13.0 μm. The second batch of samples, designated 4a-7b, were implanted with 93 MeV silver ions with charge state +19 at a mean range of 9.05 μm and a peak depth of 9.66 μm. The number of implanted ions ranged from $0.24\text{-}1.4\times10^{17}$ depending on the run conditions. Table 1 provides the details for the implantation runs.

A copper braid transferred heat from the back of the sample holder to a water-cooled copper block to provide for cooling of the samples during implantation. The temperature at the back of the samples was measured using Type K thermocouples. The measured temperature varied from 120 to 240°C during the implantation process.

The ion beam consisted of an irregular area approximately 10 mm in diameter with a 4 mm diameter central area where the ion concentration was nearly uniform. The region outside of the central region was much less uniform which resulted in variability in the as-implanted concentration profile. The entire ion beam was used for implantation directly in samples 1, 2a, and 2b. Because of this, the measured depth profiles from these samples were always taken from the center, high concentration area of the implantation. For samples 4a-7b, a mask with a 4 mm diameter hole was used to eliminate the irregular region. The ion implantation process was successful in providing a measurable silver concentration, approximately 2 atomic percent average and 20 atomic percent peak, at depths greater than 9 μm with a roughly symmetric concentration profile. This will be discussed further below. Implantation of a high silver concentration ensured that the silver concentration profile would be measurable, above the detection limits of our analysis techniques, both before and after annealing. The beam diameter and depth of the implantation in relation to the initial grain size of the SiC material assured that silver would be present both in the matrix and on grain boundaries.

TABLE 1. Ion Implantation Parameters for Silver Deposition

Sample ID	Beam Energy (MeV)	Silver Charge State	Irradiation Time (hr:min)	Time Averaged Current (eμA)	Minimum Current (eμA)	Maximum current (eμA)	Cumulative dose (atoms)
1	161	+18	11:43	1.7	1.4	2.2	2.5 E16
2a	161	+18	7:54	2.4	2.3	2.8	2.4 E16
2b	161	+18	22:17	3.2	1.5	4.8	9.3 E16
4a	93	+19	18:31	3.6	2.7	5.1	8.5 E16
4b	93	+19	20:09	5.1	4.1	8.2	1.3 E17
5a	93	+19	10:10	6.9	7.9	9.8	1.0 E17
5b	93	+19	9:21	7.6	7.0	9.0	8.7 E16
6a	93	+19	6:27	13.1	12.0	14.0	1.3 E17
6b	93	+19	6:33	12.4	12.0	13.5	1.2 E17
7a	93	+19	7:34	10.7	9.8	12.0	1.3 E17
7b	93	+19	13:21	8.7	7.2	9.8	1.4 E17

The purpose of the implantation was to provide a measurable silver distribution at a sufficient depth in the SiC to allow for meaningful annealing experiments. This goal was achieved. The implantation, however, resulted in extensive radiation damage due to the energy loss/displacement cascades developed during the process. It is thus important that questions related to the possible interaction with, and influence of, the damage and silver migration process be addressed. The radiation damage processes resulting from the slowing down of the high energy silver ions can be grouped into two general categories: (1) electronic energy loss and (2) displacement production. As a rule of thumb, the slowing down process is dominated by coulombic interactions (electronic energy loss) until the energy of the ion is reduced to approximately the atomic weight of the stopping atom in keV. Thus, for silver ions, electronic energy loss will dominate until the energy has decreased to approximately 100 keV. Roughly 95-97% of the energy loss will be in the form of heat and the majority of the heat will be deposited in front of where the displacement damage is deposited. The remaining energy loss will result in the production of displacement cascades. The displacement cascades produce damage in the form of displacements, dislocation loops, and if the dose and dose rate is high enough, amorphization and/or recrystallization of the material will occur. For the conditions of the implantations in this study, SRIM calculations indicate that significant displacement damage does not begin until a depth of 5 μm and 7 μm is reached for the 93 MeV and 161 MeV cases, respectively. The peak in displacement damage will occur at depths of about 9 μm and 13 μm, respectively. Figures 1 and 2 show the results of the SRIM calculation for 93 MeV and 161 MeV silver ions in SiC. The SRIM calculations, while using the simplified Kinchen-Pease displacement model gives a relative comparison of the number of displacements and subsequent vacancy production. The calculations are accurate when predicting the energy loss and spatial distribution of damage.

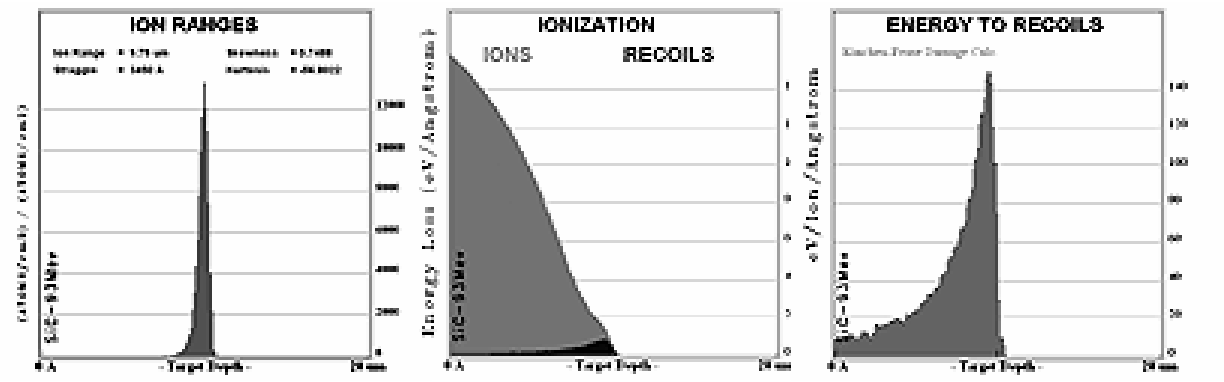

FIGURE 1. Results of SRIM calculations for silver implantation at 93 MeV.

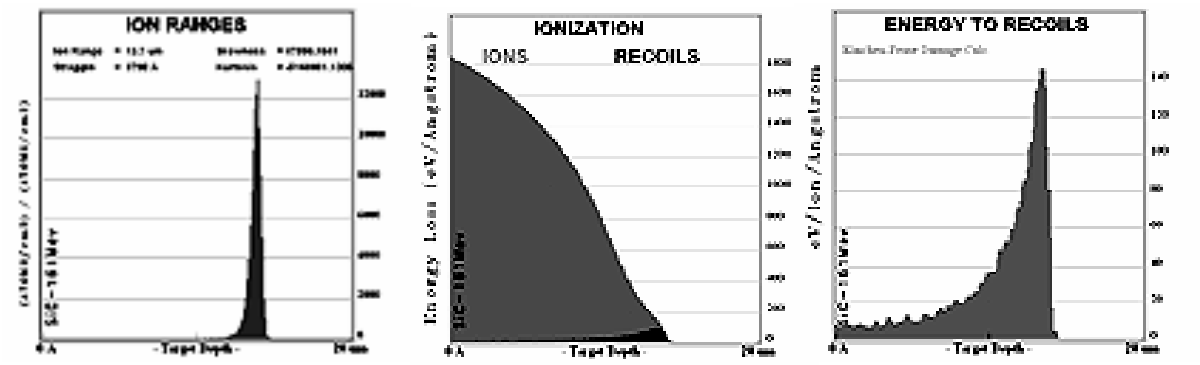

FIGURE 2. Results of SRIM calculations for silver implantation at 161 MeV.

With respect to amorphization, Wendler et al. showed that for high-energy ion damage, amorphization becomes impossible at temperatures above approximately 250°C [7]. Heera et al. have discussed the dynamic relationship between the damage rate, ion characteristics, and the location of the ion-beam induced epitaxial/amorphized region boundary [8]. Also, Pacaud et al. reported that the crystallization temperature for ion implanted SiC is approximately 950°C [9]. Based on the results of Wendler [7], Heera [8] and Pacaud, et. al [9], it was expected that the implantation process would result in a multi-zone damage region consisting of the following when proceeding from the beam entry point: (1) a region of unaltered SiC where, although the electronic energy loss deposition is very high, the displacement damage will be essentially zero, (2) a region where the displacement damage begins to accumulate which will be severely disrupted and probably crystallized, (3) a region where amorphization has occurred since the irradiation temperature was not expected to exceed 250°C, and (4) a region of undamaged SiC beyond the amorphized region which may have a diffuse boundary due to straggling of the ion slowing down process. The silver is expected to be located in the amorphous region near the boundary away from the beam entry point. With respect to the effect of the radiation damage on the morphology of the silver, as it may affect migration during subsequent annealing, the damage process will result in complete mixing of the SiC and silver in the amorphous region. Since the solubility of silver in SiC is essentially zero, we would also expect that conditions, at the concentrations expected (~2 atom % averaged over the implantation zone but of the order 20% in the peak deposition zone), would favor precipitation of elemental silver within the damage zone. At the very least, these two processes would be expected to provide an almost ideal situation in which silver is in intimate, if not actually mixed with, the SiC matrix. Additionally, the

damage produces an extensive distribution of vacancies. The expected crystallized region can also be expected to provide grain boundary area for diffusion. Lastly, the annealing process results in recrystallization of the amorphous region leading to the production of grain boundaries in the exact location of the silver. Such conditions should be ideal for migration by diffusion if this occurs. In conclusion, it is expected that the radiation damage from the implantation process would be expected to actually enhance the probability of diffusion and not hinder it.

2.3. ANNEALING CONDITIONS

After implantation, samples were annealed in a Webb graphite furnace at 1500°C for up to 480 hours. This temperature is significantly higher than typical fuel operating temperatures but is in the range of thermal treatments used for previous release-based experiments performed on irradiated fuel. This temperature was also high enough to essentially guarantee an easily measurable concentration profile change under the assumption that previously reported diffusion coefficients are accurate. Calculations of the expected profile change based on diffusion coefficients from Amain and Stöver indicated that, even for times of only several hours, the result would be essentially complete elimination of the silver from the material [5]. Annealing for 210-480 hours was, thus, expected to be more than sufficient.

The furnace environment consisted of a moderate vacuum at 1500°C with typical pressures during annealing in the range of 4-15 mTorr. Each sample was sandwiched between two blocks of silicon carbide, approximately 5 × 5 × 1.3 cm to limit interaction between the surface of the implanted SiC and any contaminants in the furnace atmosphere.

3. RESULTS AND DISCUSSION

Table 2 shows the experimental parameters and analytical methods for the implantation, annealing, and analysis. Silver concentration profiles were measured in sample 2b before and after annealing at 1500°C for 210 hours. Transmission electron microscopy (TEM) was performed on sample 6a after implantation and sample 5a after annealing for 480 hours at 1500°C to evaluate the effects of implantation and annealing on both the SiC microstructure and the silver distribution.

TABLE 2. Annealing conditions for selected samples.

Sample ID	Implanted Dose (atoms/cm^3 @ MeV)	Temperature (°C)	Time (hr)	Analysis
2b	1.9 E+21 (161 MeV)	1500	210	XPS profile
5a	2.1 E+21 (93 MeV)	1500	480	TEM
6a	2.6 E+21 (93 MeV)	n/a	n/a	TEM

3.1. SILVER CONCENTRATION PROFILES

Figure 3 shows the results of X-ray photoelectron spectroscopy (XPS) profile measurements before and after annealing at 1500°C for 210 hours. The best estimate of the errors in both position and concentration are indicated with error bars, which will be discussed below. Within the accuracy of the measurements there is no significant change in the profile after annealing.

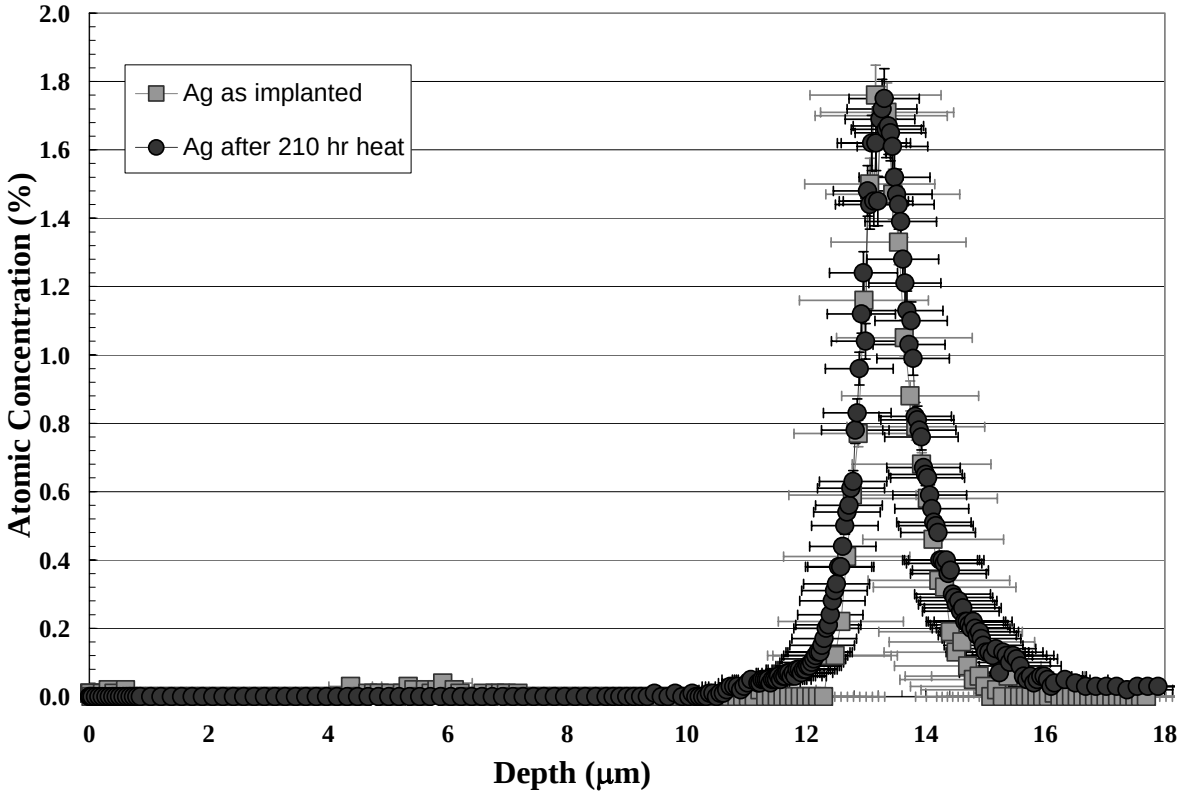

FIGURE 3. Silver concentration profiles in sample 2b before and after annealing.

3.2. ELECTRON MICROSCOPY

3.2.1 INTRODUCTION

Electron microscopy was used to characterize the SiC microstructure before and after annealing and the location of the implanted silver. Thin cross-sectional slices of two ion implantation samples, one before annealing and one after, were analyzed using scanning electron microcopy (SEM) and analytical electron microscopy (AEM).

The goal of the AEM analysis was to observe and characterize the silver location and morphology in the implanted region, both before and after annealing. An additional goal was to characterize the silicon carbide grain structure both within and outside the implantation region and also to characterize, if possible, the damage in the implanted region. The results of this analysis are shown in figures 4-9 and discussed in the following sections.

3.2.2 AS-IMPLANTED MICROSTRUCTURE

Figure 4 shows back scatter SEM micrographs of the as-implanted (sample 6a) material. Figure 4(a) shows the SRIM calculated silver profile. Figures 4(b) and 4(c) show the as-implanted microstructure at low and high magnification. The light region is the area of high silver concentration. Figure 5 shows

energy dispersive X-ray spectroscopy (EDS) results for regions labeled 1-3 in Figure 4(b). The location of the silver is consistent with the calculated displacement damage morphology shown in Figures 1 and 2.

Figure 6 shows an analytical electron micrograph (AEM) of the as-implanted SiC microstructure prior to annealing. The silver ion beam entered from the left. The as-implanted microstructure consists of a zone of altered SiC sandwiched between regions of apparently unaltered material. The altered microstructure region, however, does not completely define the extent of the implantation-induced damage. As figures 1 and 2 show, the actual damage zone extends from the entry point of the ion beam to a short distance beyond the inner-most extent of the zone of microstructural change. We would thus expect that the region of vacancy production, although peaked in the region of highest displacement damage, would actually encompass the entire region. Also, although the displacement damage zone is skewed to the right, the electronic energy loss region is skewed to the left side of the region. Thus, the region of peak heat generation rate would also be skewed to the left side of the zone.

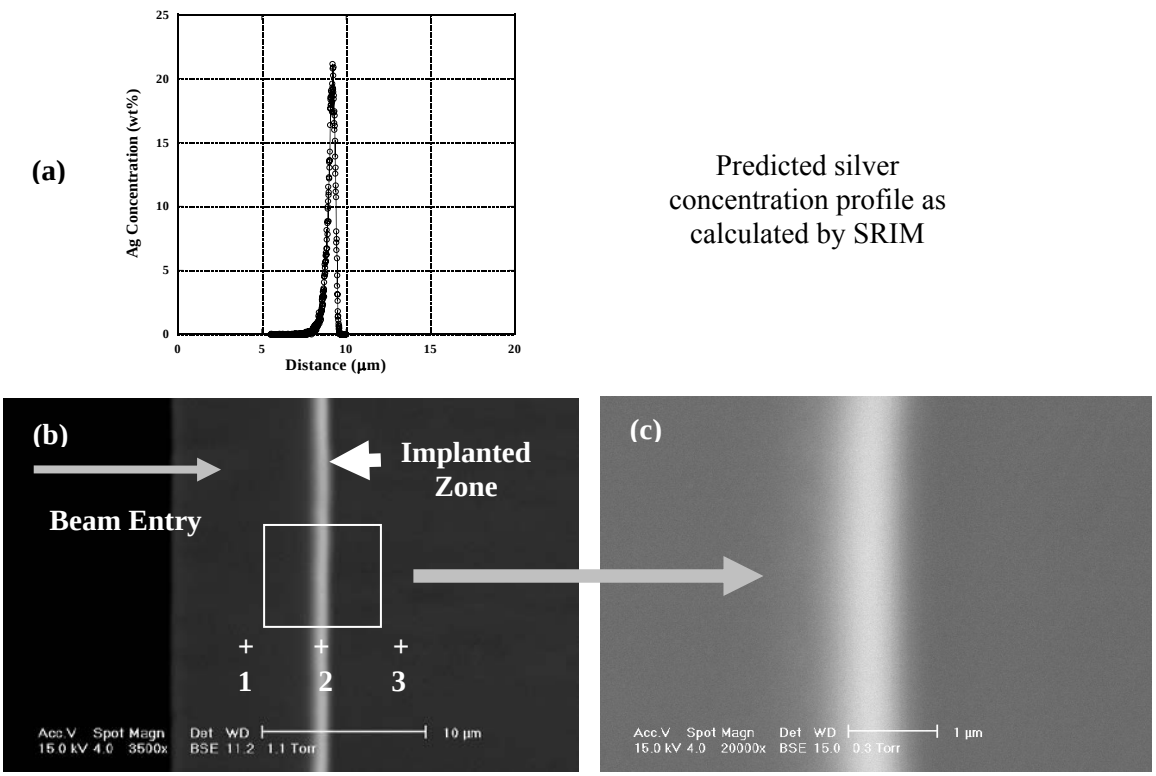

FIGURE 4. SEM micrographs showing as-implanted silver location in SiC.

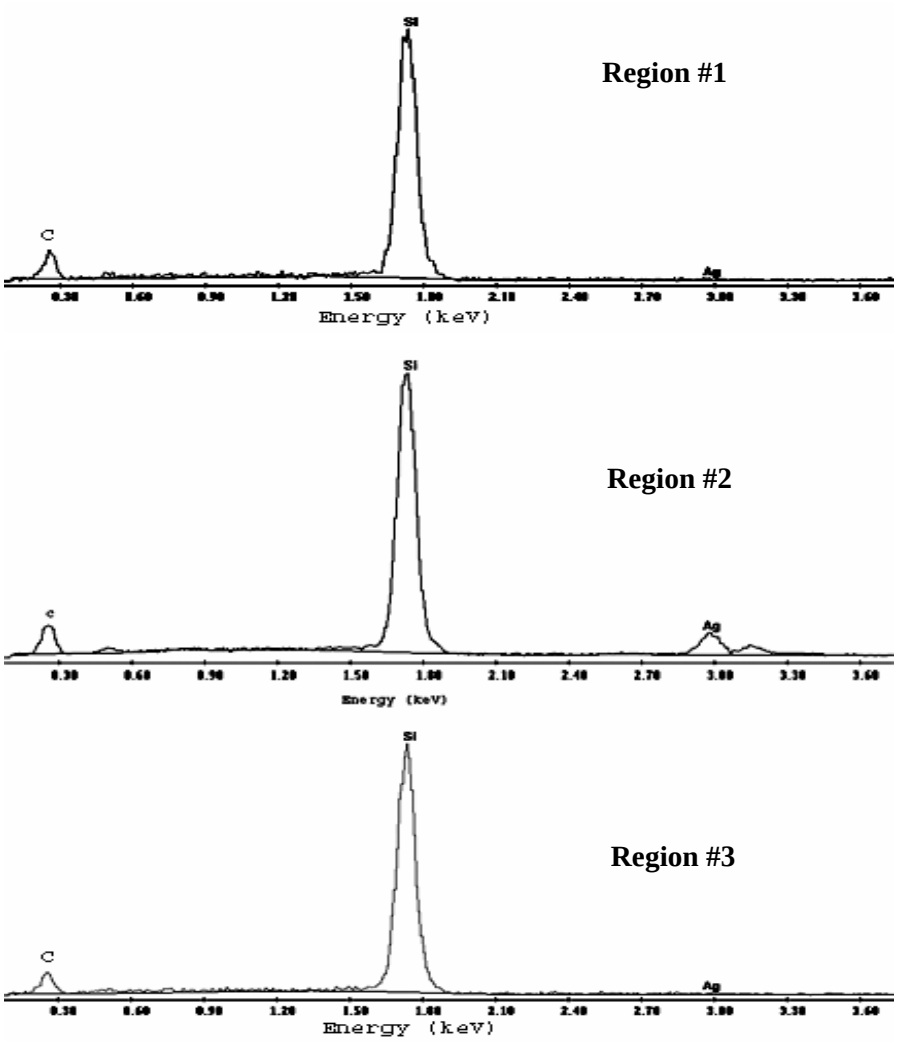

FIGURE 5. EDS spectra for as-implanted material. Silver is concentrated within a narrow band corresponding to the region predicted by SRIM calculations.

In the as-implanted microstructure, a crystallized region defines the front of the silver implantation zone. The as-fabricated silicon carbide columnar grain structure is visible to the left and right of the altered zone. The altered zone consists of three main regions. In the front-most region of the implantation zone, on the left, recrystallization has occurred. The middle of the altered zone contains an amorphous region. Towards the back, the structure is still mostly amorphous, but small crystallites have nucleated.

Although the morphology of the recrystallized region at the front of the implantation zone is fine-grained and equiaxed, there appears to be a further distinction between smaller, more equiaxed grains at the front and slightly larger, more elongated grains at the back. The smaller equiaxed grains are on the order of 50 nm to 150 nm in diameter and the larger grains are about 100-200 nm wide by 250-400 nm long.

Predicted silver concentration profile as calculated by SRIM

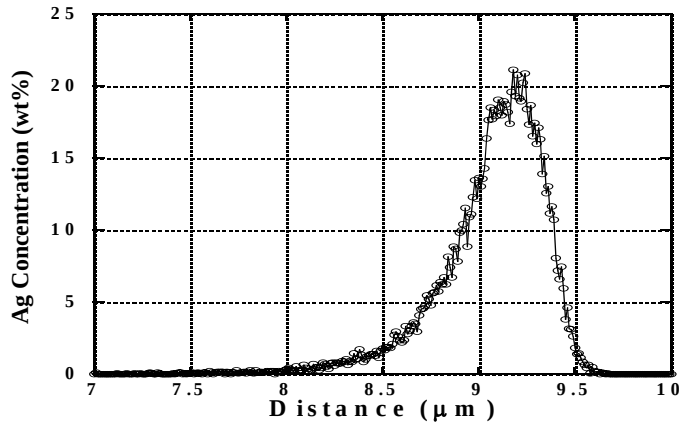

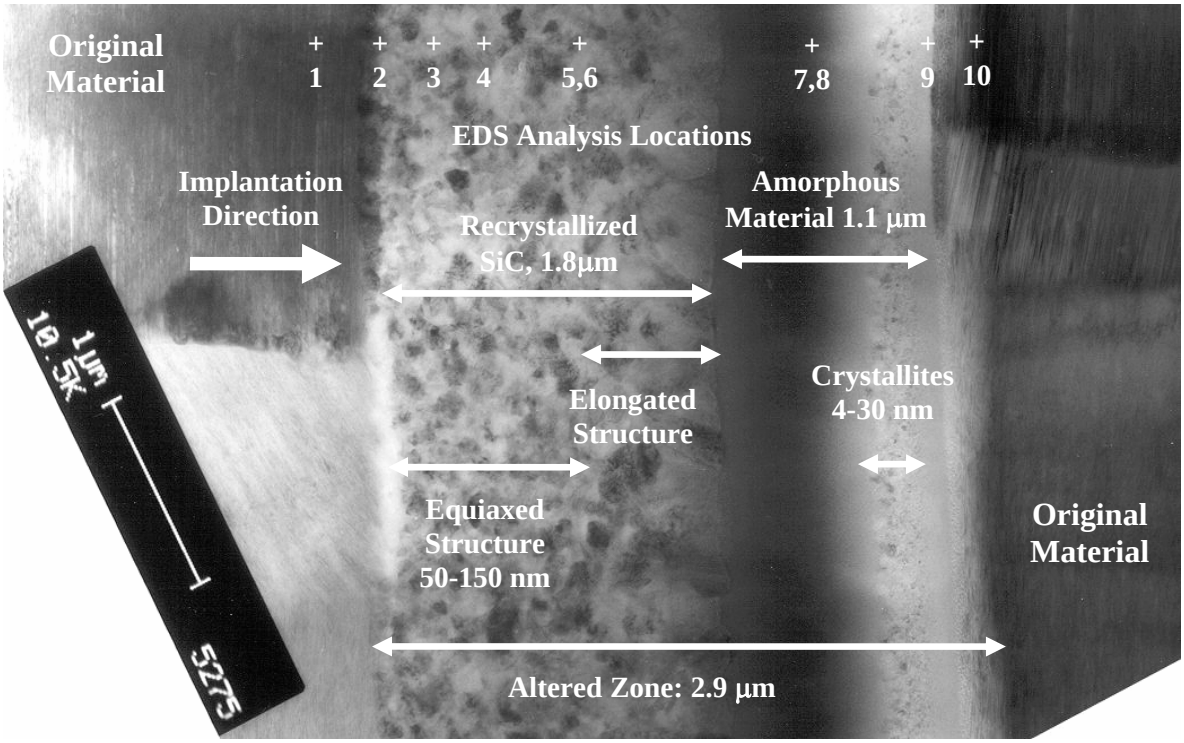

FIGURE 6. AEM micrograph of as-implanted SiC before heating.

The back 1.1 μm of the altered zone is largely amorphous, but also contains some small equiaxed crystallites ranging in size from less than 4 nm to about 30 nm in diameter. SiC grains have nucleated and started to grow in the rear of the amorphous region during implantation, but have not been able to incorporate all of the material. A thin band of the as-fabricated SiC behind the altered zone, about 300-400 nm wide, contains damage with increased faulting, though the damage was not great enough to cause amorphization or recrystallization.

Chemical analyses, using EDS, were performed along the cross-section of the implanted sample to provide a quantitative assessment, on a macro scale, of the silver concentration. The locations of EDS measurements are identified in Figure 6 and the silver concentrations are listed in Table 3. The silver profile agrees with the predicted silver implantation profile. No silver was observed in the original material in front of the altered zone or in the front portion of the recrystallized zone. Silver just above the

detection limit of 1000 ppm (0.1 atomic percent) was measured in the recrystallized zone at the boundary between the equiaxed and slightly columnar SiC grains. The peak silver concentration occurs in the amorphous region. A small amount of silver was detected at the boundary between the amorphous region and the original SiC as well as in the damaged layer of the original SiC just behind the altered zone.

TABLE 3. Most of the silver, detected by EDS, is located in the amorphous SiC region.

Spot #	Location	Relative Silver Concentration*
1	original SiC, front	none detected
2	interface between front SiC and recrystallized SiC	none detected
3	~0.2 μm into recrystallized SiC	none detected
4	in the middle of the recrystallized, equiaxed SiC	1.1
5	between the equiaxed and	2.8
6	columnar recrystallized SiC	5.1
7	amorphous damaged region	26.3
8		25.1
9	interface between amorphous SiC and original SiC	4.0
10	damage zone of original SiC	1.2

* Silver concentration in wt%. Spot # identified in Figure 6.

In addition to the AEM analysis, the as-implanted microstructure was analyzed using scanning transmission electron microscopy (STEM). The analysis was performed using a Vacuum Generators HB601 STEM at an acceleration voltage of 250 kV. The STEM allows for analysis at very high resolution. Figure 7 shows the morphology at the interface between the amorphous and recrystallized regions and Figure 8 shows the results of microchemical analysis for silver through the implanted region.

At this resolution it is clear that the silver morphology depends on the specific region within the altered zone. In the amorphous region the silver is separated into small, approximately 5 nm diameter, regions. The distribution of these regions is random, in keeping with the amorphous nature of the SiC. In the recrystallized material the silver size is slightly larger but the morphology is now oriented within the crystal structure. β-SiC (3C-SiC) crystallizes in the zinc blende structure which can be visualized as two interconnecting (carbon and silicon) face centered cubic lattices. The morphology of the silver suggests a preference for precipitation on the close packed planes in this structure. Figure 8 shows an elemental line scan through the amorphous region generated using the STEM. The results, although qualitative, confirm that the silver is located primarily within the amorphous region.

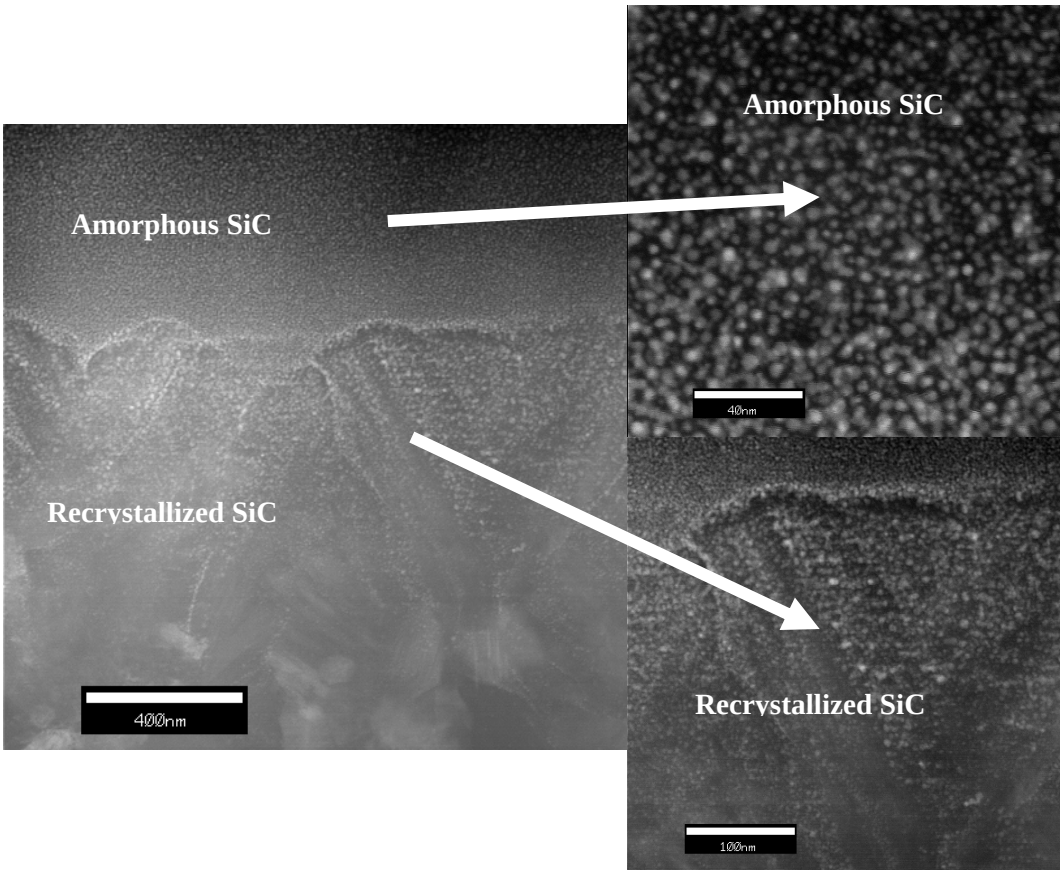

FIGURE 7. STEM micrographs of as-implanted SiC showing the region at the interface between the amorphous and recrystallized regions.

3.2.3 ANNEALED MICROSTRUCTURE

Figures 9-14 show the microstructure of the annealed (480 hours at 1500°C) material. Figure 9 shows a set of SEM back scatter images at increasing magnification. A comparison of Figure 9 with Figure 4 shows that the morphology of the silver coarsened during the anneal. Moreover, it appears that preferential precipitation has occurred in some regions as the brighter localized regions in the right side of Figure 9a show. Figure 10 shows a STEM micrograph and silver map for the annealed material. The silver has clearly remained segregated within the implanted region.

Figures 11-13 show TEM micrographs of the annealed microstructure. Figure 11 shows the microstructure of the entire implanted region. The implantation zone completely recrystallized, as expected. This is shown more clearly in Figure 12. The amorphous SiC was completely eliminated in the altered zone after annealing. The recrystallized zone is approximately 2.1 μm wide and is characterized by two regions. The front region, which closely corresponds to the region formally crystallized during the implantation process, has been transformed into an epitaxial, columnar region. The formally amorphous region has crystallized and is characterized by a fine equiaxed structure. The back half of the recrystallized zone also contains precipitated silver regions, phase separated from the silicon carbide. The silver appears darker than the SiC due to its higher atomic number. The silver is segregated from the SiC and has accumulated between grain boundaries.

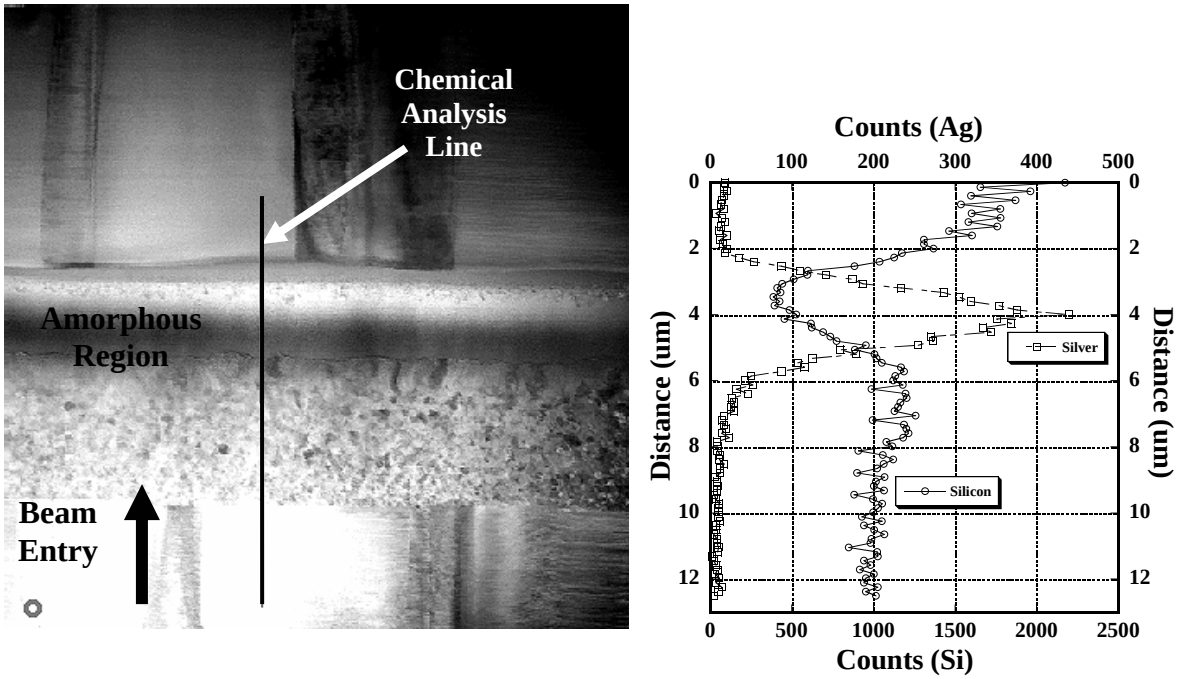

FIGURE 8. STEM analysis for silicon and silver. The silver concentration peaks in the amorphous region.

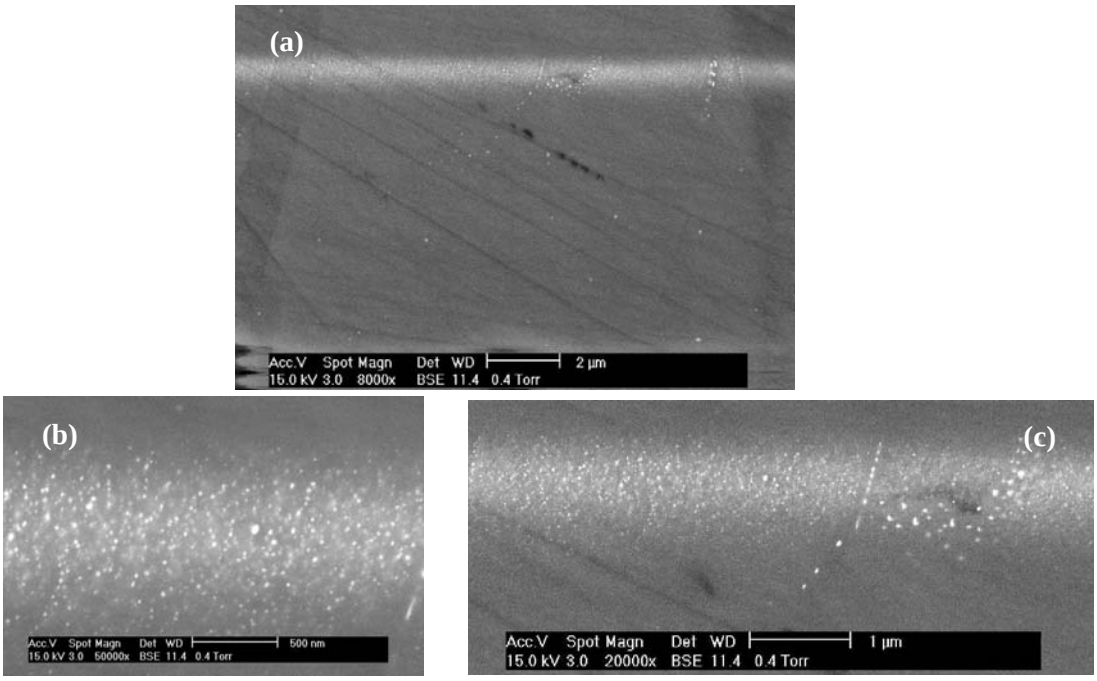

FIGURE 9. SEM back scatter image of the annealed microstructure.

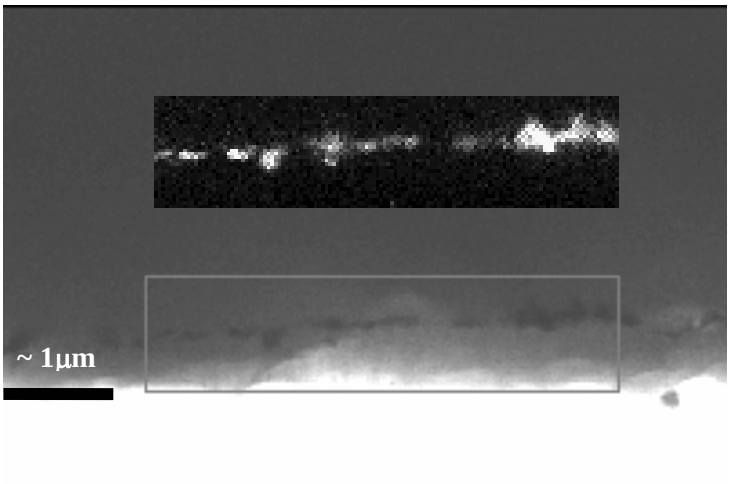

FIGURE 10. STEM micrograph with silver element map showing silver location after annealing at 1500°C for 480 hours.

Figures 13 and 14 show TEM micrographs of the annealed microstructure, focusing on the area immediately behind the recrystallized region. In this region, the implantation damage was not sufficient to cause either crystallization or amorphization of the original microstructure. The radiation damage calculations, however, indicate that a significant amount of displacement damage should have been present. Small precipitates of silver decorate the silicon carbide behind the recrystallized zone. These silver precipitates are approximately 4-20 nm in size. The layer is approximately 300-400 nm wide. Silver is only present in the damaged region and does not appear in the undamaged, as-fabricated SiC. Figure 14 shows the details of a typical grain boundary region. Extensive analysis of the grain boundaries in the region immediately behind the damaged region, where grain boundaries from the undamaged region intersect the damaged, silver-containing region, could not detect the presence of silver. Silver has not diffused into the undamaged SiC regions in spite of the fact that optimum conditions existed in this region for diffusion to have occurred.

4. DISCUSSION

4.1 COMPARISON OF AS-IMPLANTED AND ANNEALED BEHAVIOR

The implantation process resulted in the creation of both crystalline and amorphous regions in the CVD SiC microstructure. These two processes would have resulted in extreme mixing of the SiC structure. At the same time, the solubility of silver in SiC is negligible. Thus, at the concentrations implanted in this study, approximately 2 atom % averaged, the observation of phase separated silver over a very narrow damaged region was not unexpected. Nevertheless, from the standpoint of establishing the initial conditions for the study of migration of silver in SiC, this process achieved its goal. The as-implanted microstructure contained silver in intimate contact with the SiC both in the matrix and in immediate proximity to grain boundaries.

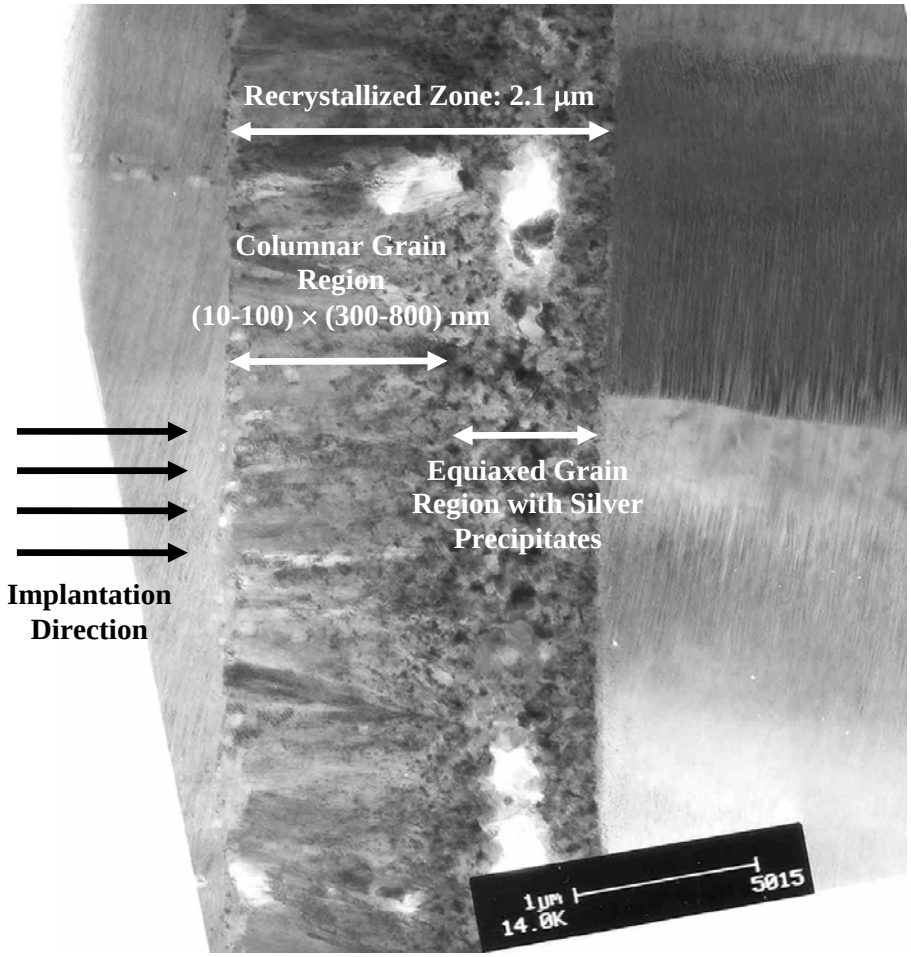

FIGURE 11. TEM micrograph of as-annealed material after 480 hr @ 1500°C.

The recrystallization process created new grain boundaries as well as a significant increase in grain boundary area relative to the original CVD SiC microstructure. As the amorphous SiC crystallized to form β-phase grains, impurity silver atoms were rejected due to their low solubility. The change in morphology of the silver is clearly evident in the SEM micrographs in Figures 7 and 9. The silver atoms segregated from the recrystallized SiC grains and continued to appear as phase-separated precipitates in the recrystallized zone. During the annealing process the silver had intimate access to the SiC grain boundaries, however, no silver migration was observed either by XPS or AEM analyses. A region of low-concentration silver exists just behind the recrystallized SiC in the heavily faulted original SiC microstructure yet, there is no evidence of silver migration along grain boundaries present in the original SiC. If grain boundary diffusion is the most likely mode of migration, it should have been evident in this region.

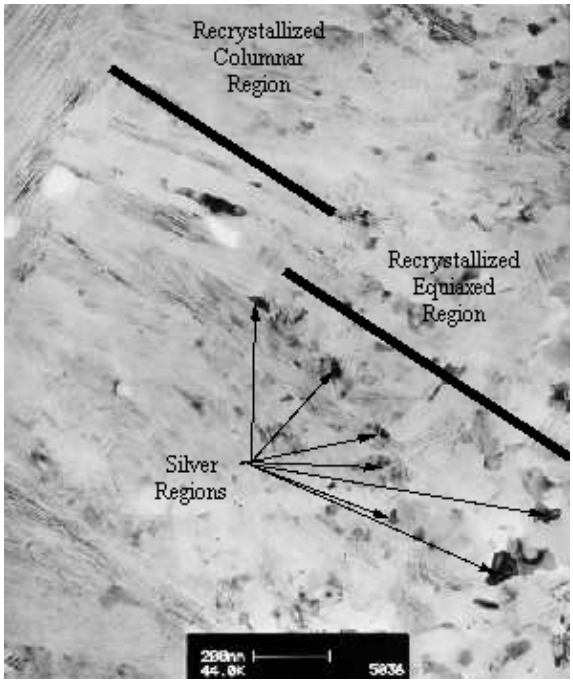

FIGURE 12. Detail of recrystallized region after annealing showing typical areas where silver was detected.

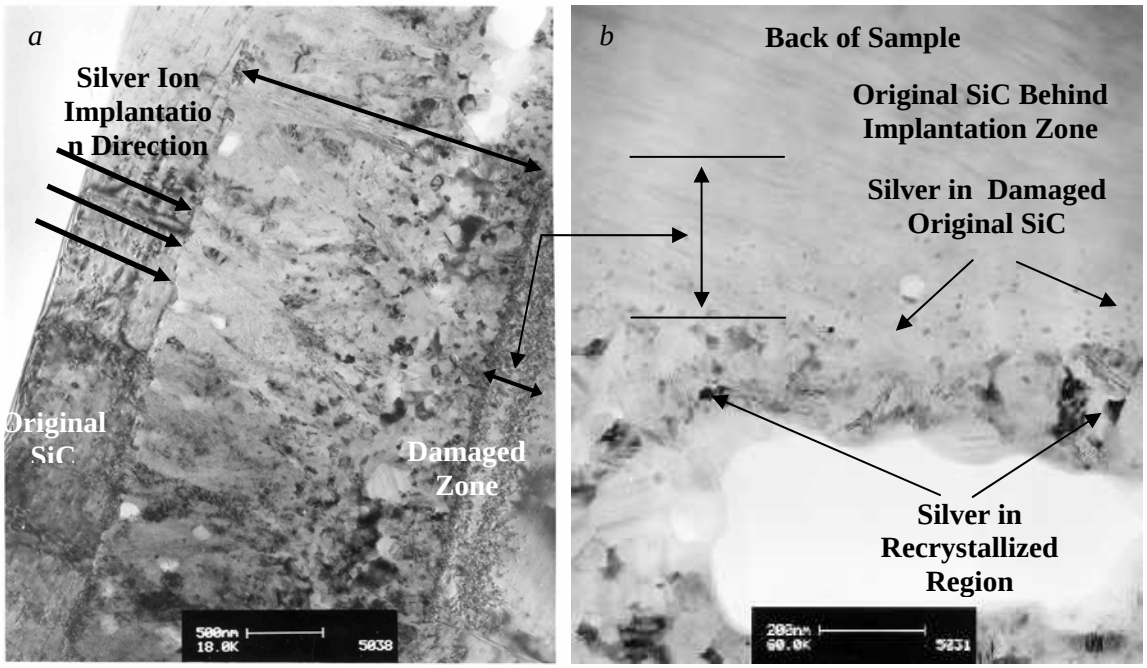

FIGURE 13. AEM micrograph series of annealed material showing details of region behind the recrystallized region.

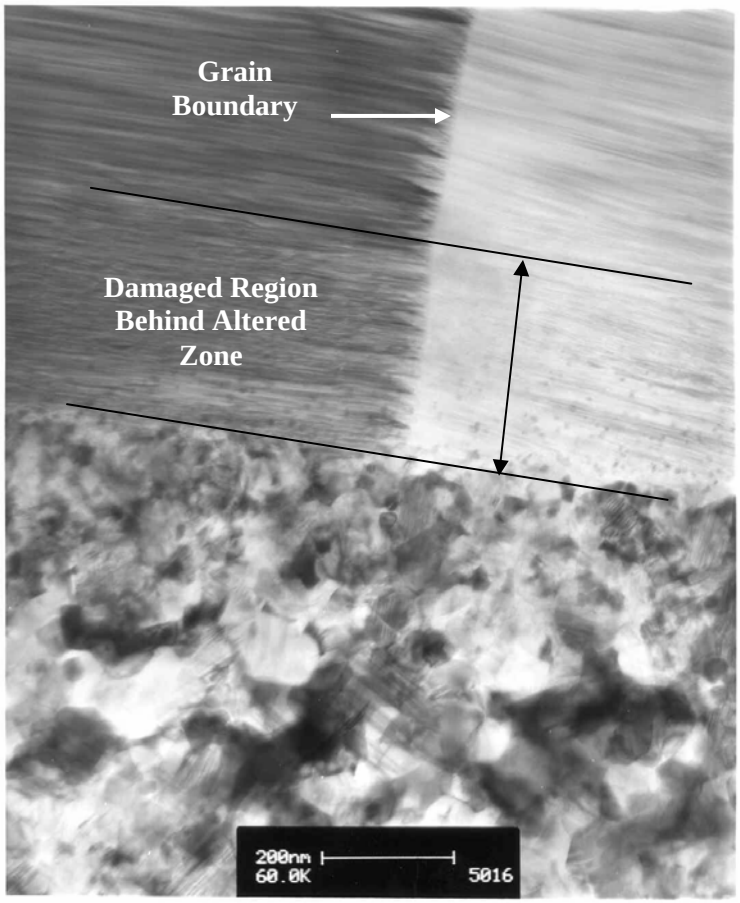

FIGURE 14. AEM micrograph showing details of a SiC grain boundary at the interface between damaged and undamaged regions after annealing for 480 hours at 1500°C. No silver could be detected on grain boundaries.

With respect to the question of the effect of radiation damage on potential introduction of "artifacts" in the diffusion process, consider the shape of the concentration profile before and after annealing. The supersaturation of vacancies that would have existed as a result of the implantation process should have, along with the formation of extended defects such as loops or voids, also provided for enhanced diffusion in the damaged region but not in the undamaged region. Rough calculations indicate that the vacancy production rate in the peak damage region would have been of the order 10^{21} vacancies/s/cm^3. The vacancy production rate would have tailed off toward the beam entry region but would still have been significant. The vacancy production rate, however, would have tailed off much more abruptly beyond the peak damage region and would have been zero in the region beyond the damaged region. Since the implantation temperature was far below any temperature for which vacancy migration would have been significant, the vacancy concentration would have been very high prior to annealing. This would have greatly enhanced the recrystallization process yet, inspection of the shape of the concentration profile shows that there is little, if any, change in the shape resulting from the annealing process.

4.2 COMPARISON TO LITERATURE

In a previously reported ion implantation experiment, Nabielek et al. did not observe silver diffusion. Nabielek et al. implanted lower energy silver ions into silicon carbide, just below the surface, and annealed the sample for only 30 minutes at 1180°C [1]. Rutherford backscattering measurements before and after annealing showed no change in the silver concentration profile. The authors concluded that silver had most likely been trapped in SiC grains and, therefore, silver diffusion was not observed because matrix diffusion of silver in SiC is much, much slower than grain boundary diffusion. Early results from this program have also indicated that migration by diffusion does not occur [3,4]. Recent results from Jiang et al., who implanted 6H-SiC with 2 MeV Si ions followed by annealing at 1300°C, support this observation [10].

The results of this work suggest that, while trapping of some silver in the SiC matrix may be occurring, immobilization of silver at SiC grain boundaries is also likely occurring. The solubility of silver in silicon carbide is extremely low, as these results confirm, and silver was swept from the grains during recrystallization yet no change in the shape of the concentration profile was observed.

In another study of the retention of silver in coated particle fuel, Nabielek observed (as have others) a large variability in the retention of silver for nominally identical conditions [11]. He postulated that one possible explanation for the observed behavior is that migration of silver is enhanced by the presence of free silicon on the grain boundaries. No evidence was offered to support this hypothesis. XPS results from this work did not show the presence of free silicon although the sensitivity of the analysis was only approximately 0.1 atomic % for free silicon.

Another possibility for a rationalization of the difference between release-based diffusion measurements, their high variability, and the results of this work might be that the release is due to an entirely different mechanism. One mechanism could be vapor transport through "nano" cracks that are either present from the fabrication or are generated during thermal and irradiation exposure. Recent results using specially prepared spherical diffusion couples, where the silver was encapsulated within a sphere of SiC, appear to show the same variability in release that has been observed with actual fuel particles[12]. To the accuracy of the chemical analysis performed to date, no silver has been observed within the SiC after annealing in the 1200-1700°C temperature range. Additionally, helium leak testing of samples before and after heating has shown an increase in leak rates [12]. Since helium leaks can only occur if mechanical paths are present, this gives support to the possibility that vapor transport may be playing a role.

Also important to note is that the final recrystallized SiC grain structure for the results reported here is similar to that fabricated in typical SiC layers in tested TRISO-coated particle fuel. Although there are differences between some of the coating parameters, the SiC used in the current experiments and the SiC from previous fuel tests were coated using the same high temperature CVD process which resulted in high-density β-SiC with a fine-grain structure. Figure 15 shows the microstructure that is typical of TRISO-coated SiC fuel [13]. This microstructure should be compared with the equiaxed microstructure shown in Figure 14. The two microstructures are quite similar. This similarity suggests that these results are applicable to the case where silver release is occurring in TRISO-coated particle fuel.

5. CONCLUSIONS & IMPLICATIONS

The results of this work show that silver did not move by diffusion, either in the matrix or along grain boundaries, in SiC for the conditions studied. Migration by diffusion could actually be occurring. However, if the assumption is made that migration was actually occurring but in amounts just below the minimum sensitivity of the analysis then the diffusion coefficient would have to be less than 5×10^{-21} m^2/sec.

The silver concentration used in this work is far above that which would be expected to exist in TRISO-coated particle fuel. The annealing temperature for this work, however, is in the same range as the post-irradiation annealing studies used to derive diffusion coefficients for coated particle fuel. Additionally, the microstructure of the SiC used in this work is either similar to TRISO-coated particle fuel SiC or of a structure that should have enhanced the resulting silver migration behavior. We thus conclude that these results are applicable to the case of silver migration in CVD SiC for coated particle fuel.

The results of this work are significant with respect to approaches that might be applied to the mitigation of silver release in coated particle fuel. If, as has been previously assumed, release is by diffusion then little can (or could) be done to mitigate release short of changing to a more resistant material. However, if silver does not diffuse in silicon carbide, then silver release from coated particle fuel must be controlled by transport along another path. These results indicate that the path may be more mechanical then microstructural although it is likely that microstructure would play a critical role in allowing mechanical paths to develop. However, under these circumstances additional work may both identify the actual path and then point to ways of reducing the probability of this path from developing.

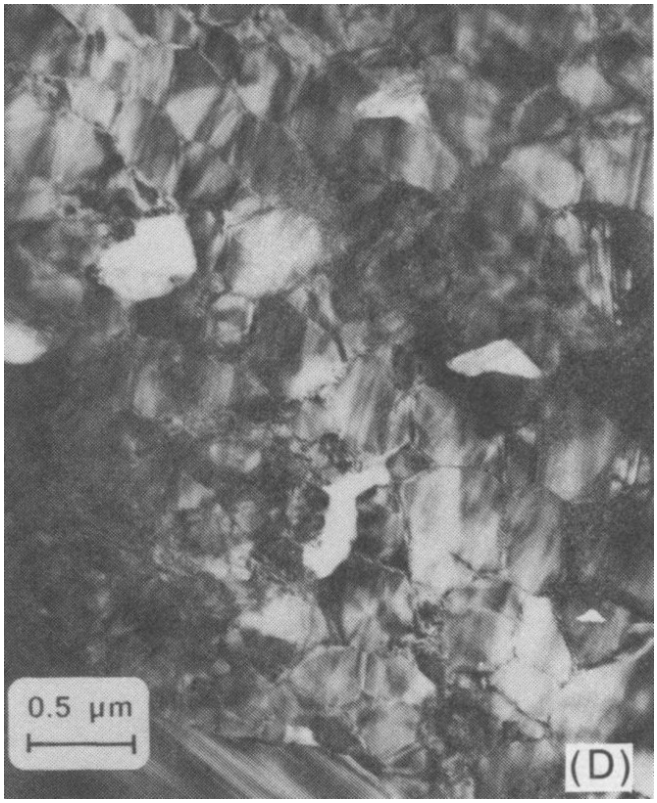

FIGURE 15. Comparison of typical CVD SiC microstructures [13].

REFERENCES

[1] H. Nabielek, P. E. Brown, and P. Offerman, "Silver Release from Coated Particle Fuel," *Nucl. Tech.*, **35** (1977) 483-493.

[2] J. Bernhok, S. A. Kajihara, C. Wang, A. Antonelli, and R. F. Davis, *Mater. Sci. Eng. B* **11** (1992) 265-272.

[3] H. J. MacLean, and R. G. Ballinger, "Silver Migration and Release in Thin Silicon Carbide," ANS Annual Winter Meeting, Washington, DC, November 2002.

[4] H. J. MacLean and R. G. Ballinger, "Silver Migration in SiC: A New Perspective", ANS Global 2003, New Orleans, LA, November 17-20, 2003.

[5] W. Amian and D. Stöver, "Diffusion of Silver and Cesium in Silicon-Carbide Coatings of Fuel Particles for High-Temperature Gas-Cooled Reactors," *Nucl. Tech.* **61** (1983) 475-486.

[6] The Stopping and Range of Ions in Matter (SRIM) J. F. Ziegler, and J. P. Biersack (www.SRIM.org), Copyright (1984, 1986, 1989, 1994, 1998, 2003).

[7] E. Wendler, A. Heft, and W. Wesch, "Ion-Induced Damage and Annealing Behavior in SiC," *Nucl. Instr. Meth. B* 141 (1998) 105-117.

[8] V. Heera, T. Henkel, R. Kogler, and W. Skoroupa, "Evidence for Diffusion-Limited Kinetics of Ion-Beam-Induced Epitaxial Crystallization in Silicon," *Phys. Rev. B* **52** (1995) 776.

[9] Y. Pacaud, J. Stoemenos, G. Brauer, R. A. Yankov, V. Heera, M. Voelskow, R. Kogler, and W. Skorupa, *Nucl. Instr. Meth. B* **120** (1996) 177.

[10] W. Jiang, W. J. Weber, V. Shutthanadan, L. Li and S. Thevuthasan, "Thermal and Dynamic Responses of Ag Implants in Silicon Carbide," *Nucl. Instr. Meth. B*, **219** (2004) 642-646..

[11] H. Nabielek, "The Mechanism of Silver Retention in Coated Particle Fuel," DPTN/801, O.E.C.D. High Temperture Reactor Project, Kernforschungsanlage Julich, A.E.E. Winfrith, Dorchester, Dorset, England, April 1976.

[12] H. J. MacLean, "Silver Transport in CVD Silicon Carbide", PhD Thesis, MIT, Department of Nuclear Engineering, June 2004.

[13] C.H. Carter, Jr., R.F. Davis, and J. Bentley, "Kinetics and Mechanisms of High-Temperature Creep in Silicon Carbide: II, Chemically Vapor Deposited," *J. Am. Ceram. Soc.* **67** (1984) 732-740.